Magnetic Field Enhancement of Water Evaporation in Confined Spaces

Sruthy Poulose[1] [ID] , Yara Alvarez-Braña[2,3] [ID] , Lourdes Basabel-Desmonts[3,4],
Fernando Benito-Lopez[2] [ID] , and John Michael David Coey[1*] [ID]

[1] School of Physics, Trinity College, Dublin 2, Ireland
[2] Microfluidics Cluster UPV/EHU, Analytical Microsystems and Materials for Lab-on-a-Chip Group, Analytical Chemistry Department, University of the Basque Country, 01006 Vitoria-Gasteiz, Spain
[3] Microfluidics Cluster UPV/EHU, BIOMICs Microfluidics Group, Lascaray Research Center, University of the Basque Country, 01006 Vitoria-Gasteiz, Spain
[4] IKERBASQUE, Basque Foundation for Science, E-48013 Bilbao, Spain
* Life Member, IEEE

Abstract—Water is studied in confined environments where it evaporates into its own vapor. Simultaneous experiments are conducted for 0.4–0.5 µL droplets confined at the center of 54 mm long microchannels with a cross section of 0.38 mm^2 in the presence and absence of a 300 mT magnetic field. Results are compared with those for water in half-filled 100 mL beakers. The magnetic enhancement of the evaporation rate is much greater in the microchannels, where effects range up to 140% even though the air is saturated with water vapor, as compared to $12 \pm 7\%$ in a 500 mT field in the beakers. The average steady state, no-field evaporation rate of 0.13 kg·m^{-2}·h^{-1} in the microchannels is roughly double that in the beakers, but less than the value expected at an open surface in still air. The magnetic enhancement is analyzed in terms of the *ortho* and *para* nuclear isomers of water vapor, which behave as independent gasses. The *ortho:para* ratio in fresh vapor is close to 2:3, and quite different from the 3:1 equilibrium ratio in ambient air. Evaporation is increased by the gradient of the applied magnetic field, which dephases the Larmor precession of the two proton spins of hydrogen in a water molecule and tends to equalize the isomeric populations in the vapor, thereby increasing the evaporation rate.

Index Terms—Magnetochemistry, evaporation of water in magnetic field, *ortho* and *para* water vapor, microfluidic channels.

I. INTRODUCTION

Many claims have been made for the effects of a magnetic field on the physical properties of water [Chibowski 2018]. These include an enhancement of the evaporation rate in a static field that has been measured in different ways [Nakagawa 1999, Chibowski 2014, Duenas 2021, Yang 2021], but its molecular origin is often perplexing. It has been suggested that the magnetic field somehow modifies the network of molecular hydrogen bonding in water, but there is no agreed explanation of how this is possible. The decrease of energy in an applied field B is $0.5\chi_{mol}B^2/\mu_0$, where the molar susceptibility of water is -1.6×10^{-10}. In 1 T this is -64 µJ·mol^{-1}, eight orders of magnitude less than the hydrogen bond energy (23.3 kJ·mol^{-1}). The influence of magnetic fields in magnetochemistry is usually not a thermodynamic effect, but a quantum mechanical effect, related to a change of symmetry of the wavefunctions.

In a recent study [Poulose 2023], we reviewed existing literature and then monitored the evaporation simultaneously from two beakers half filled with water that are kept in the same environment, one in a 500 mT field and the other a zero-field control [see Fig. 1(a)]. Thirty-six runs of 16 or 60 h established a systematic $12 \pm 7\%$ increase of evaporation rate in the presence of the field. By analogy with the *ortho* and *para* isomers of hydrogen gas, where the total nuclear spin I of the two protons in a H$_2$ molecule is respectively 1 or 0 [Abragam 1961], the field effect in H$_2$O was explained by treating the *ortho* and *para* nuclear isomers of water

vapor as quasi-independent gases. It is very challenging to separate and preserve *ortho* and *para* liquid water [Mammoli 2015], but in vapor, the two isomers do not equilibrate for weeks [Chaplin 2021]. We found that the *ortho* fraction in freshly evaporated vapor was $39 \pm 1\%$, compared to 75% expected from the equilibrium 3:1 *ortho:para* ratio in ambient air that has been confirmed experimentally by terahertz spectroscopy [Mamrashev 2018]. A magnetic field changes the evaporation rate because it alters the isomeric ratio in the vapor, either by dephasing the nuclear Larrmor precession of the two protons in the field gradient or by Lorentz stress in the field [Poulose 2023]. Here, we report and analyze a greatly enhanced influence of a magnetic field on evaporation rate when the water is confined in a microfluidic channel.

II. EXPERIMENTAL METHOD

The channels are made from three layers of poly(methyl methacrylate) (PMMA). The microfluidic chips are assembled by thermo-lamination after cutting a 1 mm wide channel, 54 mm long in the 0.38 mm thick middle layer with a CO$_2$ laser. A schematic image of the experimental arrangement is shown in Fig. 1(b). Two chips are used in each experiment. No magnetic field is applied to the control chip, while the other chip is exposed to a field of 300 mT produced by rectangular 50 mm × 20 mm × 10 mm Nd-Fe-B permanent magnets with a remanence of 1.26 T. They are magnetized along the short axis and used to create a field in a direction perpendicular to the channel. The evaporation of water in the two chips is monitored simultaneously using PCE800mm USB cameras. Channels are prewetted prior to the measurements by introducing 0.6–0.7 µL of Millipore deionized water
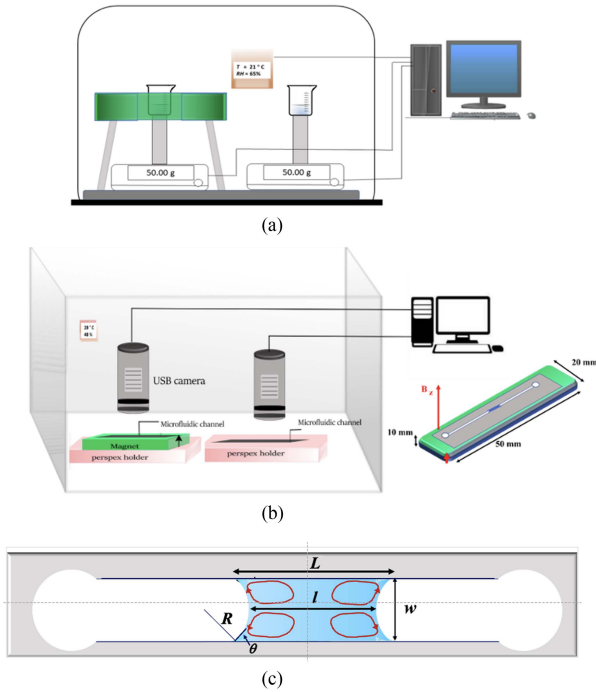
Fig. 1. Experimental arrangements to monitor (a) the weight loss by evaporation of water in half-filled beakers [Poulose 2023] and (b) the volume loss by evaporation of water in microfluidic channels in the present experiments. In each case, measurements are made simultaneously on two samples, one with the water in a magnetic field produced by permanent magnets (green) and the other a no-field control. (c) Definitions of the dimensions of a sample of water in the microchannel. The menisci are due to periodic variation of the channel width caused by laser cutting, which is evident in Fig. 2.

at one end and drawing it through the channel with a syringe pump. Then another droplet of about 0.4 μL is introduced into each prewetted channel and drawn to the center using the pump. The two ends of each microchannel are left open to ambient air, and the evolution of the shapes of the drops in the two channels is recorded as they shrink down to a membrane after several hours and rupture shortly afterward. The twin setup was enclosed in a perspex box. The ambient temperature (26 °C) and relative humidity (RH) (42%) in the laboratory were controlled throughout.

After moving a 0.4 μL droplet to the center of a channel, two menisci soon form at the edges with contact angles θ of about 30°, as seen in Fig. 2. Water normally exhibits a contact angle < 90° on PMMA [Zhang 2014], but the main reason for the menisci to form is the periodic variation of the channel width due to cutting with the CO_2 laser. The variation is 10% of the 1 mm width, and the period is 300 μm. Just like a soap film or a magnetic domain wall, the water surface seeks to minimize its area and form a circular meniscus because of surface tension. The contact angle at the laser-cut edges oscillates during the evaporation measurement as a meniscus jumps to a neighboring pinning point in a stick-slip process. The contact angle at the upper and lower PMMA surfaces is close to 90°. The volume of water remaining in the confined drop is obtained directly from its approximately symmetric shape, which is parameterized by L, the average of contact lengths at the two edges and l, the shortest distance between the centers of the two menisci, as shown in Fig. 1(c). The volume V of liquid is calculated from L and l knowing the width w and the depth d of the channel.
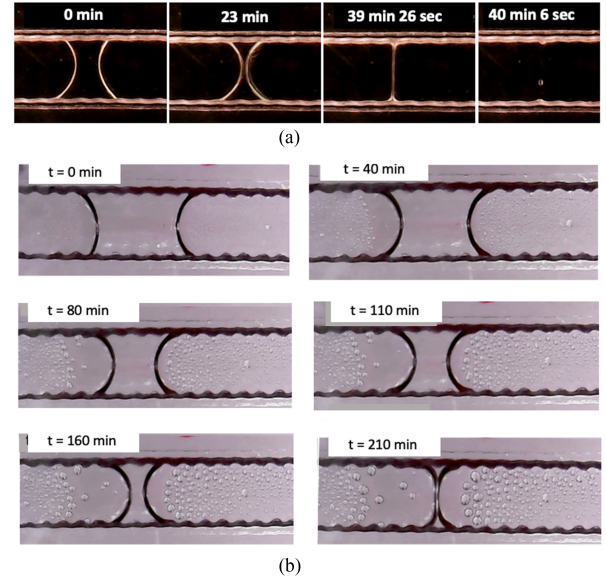

Fig. 2. (a) Evolution of 0.12 μL drop of water in a microfluidic channel. It shrinks in 39 min to leave a membrane that ruptures 30 s later. (b) Typical example of evaporation of a 0.5 μL drop. Growing sessile droplets of recondensed water vapor are seen forming in the channel beyond the menisci in the presence of the applied field, indicating that relative humidity there is 100%.

The radius of curvature R of the menisci is related to L, l, and w by the intersecting chords theorem

$$R = \tfrac{1}{4}\left[w^2/(L-l) + (L-l)\right]. \qquad (1)$$

The area A of each meniscus, $2Rd(\pi/2 - \theta)$, is

$$A \approx 2Rd\sin^{-1}(w/2R) \qquad (2)$$

and a good approximation for the volume of water spanned by the meniscus for a wide range of contact angle $20° < \theta < 60°$ is $w^2 d\theta/3$. Hence, the volume of the whole drop of water is

$$V \approx wd(L - 2w\theta/3). \qquad (3)$$

The contact angle θ is $\tan^{-1}[(2R-L+l)/w]$. For example, the volume of a sample of water with $L = 2$ mm in the channel of width $w = 1$ mm and depth $d = 0.38$ mm is 0.51 μL, when $\theta = 0.5^c$ (29°). R is 0.57 mm, and $l = 1.4$ mm.

III. RESULTS

Images of the water in both channels were recorded at five-minute intervals, and two examples of drops evolving as the water evaporates are shown in Fig. 2. Fig. 2(a) captures the last moments of a sample of water at the center of the channel that shrinks to a membrane, and then ruptures. Fig. 2(b) shows a typical, larger sample that takes almost 4 h to evaporate. Sessile droplets of recondensed water vapor can be seen growing in the channel beyond the menisci. Other images show the menisci jumping from one pinning point at the edge to a neighboring point as evaporation proceeds. The images of the evaporation in-field resemble those in no field. The curved shape of a meniscus helps to increase the evaporation rate, but the meniscus area, from which evaporation is occurring, remains roughly constant and equal to $2wd$.

Data shown in Fig. 3 are for two representative runs, where the water takes about four hours to evaporate without a field. Initial values of L and l are normalized to 1. The in-field evaporation is notably faster.
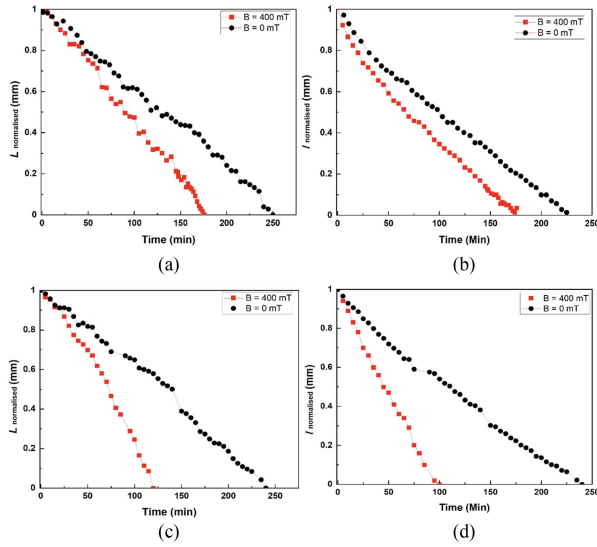
Fig. 3. Variation of L and l, normalized to the values at $t = 0$, during two evaporation experiments. (a), (b) Experiment 1. (c), (d) Experiment 2. Data in black circles are for the no-field channel, and data in red squares are for the channel in a 300 mT magnetic field.

The variation of L shows steps related to discontinuous jumps of the menisci from one pinning point to the next, but the time-dependence of l is smoother.

Ten runs were analyzed. The results, like those obtained in beakers, showed significant variability. The average evaporation rate from the control channel was 0.13 ± 0.03 kg·m^{-2}·h^{-1}, and the magnetic field enhancement of the evaporation rate ranged up to 140%, with an average of $61 \pm 42\%$. The stable sessile droplets of water with diameters of 30–150 μm growing slowly in the channel throughout a run were observed in the channel with the magnetic field. Probably a result of the enhanced evaporation rate, they appear at distances greater than about 100 μm from the menisci in Fig. 2(b), which means that the air in the microchannel at 299 K must be saturated with water vapor. Sessile droplets in arrays are known to evaporate faster in confined conditions in unsaturated air if they are located at the edge of the array than if they are surrounded by other droplets [Davoust 2013]. Here we observe the opposite effect of droplet growth in saturated vapor.

IV. DISCUSSION

A useful starting point for discussing evaporation of water is an empirical expression used by engineers for the evaporation rate in kg·m^{-2}·s^{-1} from swimming pools or other open surfaces in still air [Engineering Toolbox 2004]

$$g = Q x_{\mathrm{sat}} (1 - \mathrm{RH}). \tag{4}$$

The prefactor Q is 25 kg·m^{-2}·s^{-1}. (In an airflow of v ms^{-1} Q becomes $25 + 17v$). x_{sat} is the dimensionless saturation concentration of water vapor in air in kg/kg, which depends strongly on temperature, as shown in Fig. 4. Numerically, it is almost equal to the quantity c_{sat}, in kg·m^{-3} since the density of air is approximately 1 kg·m^{-3}. RH is the fractional relative humidity. Taking RH $= 0.5$ and the value of x_{sat} at 295 K as 0.02, we obtain $g = 0.250$ kg·m^{-2}·s^{-1}. Results for the steady-state evaporation rate of deionized water (at $t > 1$ h) for a series of runs from beakers at different values of ambient relative humidity are collected in Fig. 5. The data are consistent with the $(1 - \mathrm{RH})$ dependence of (4), but the value at RH $= 0.5$, for example, is $g =$
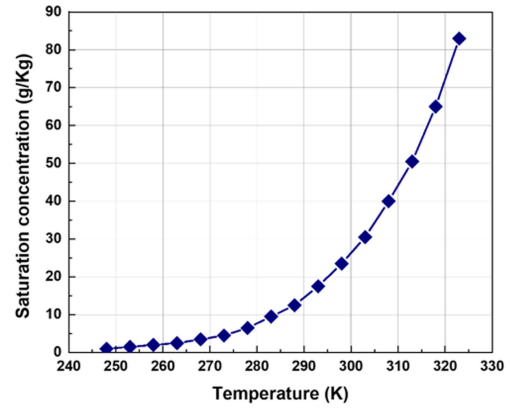

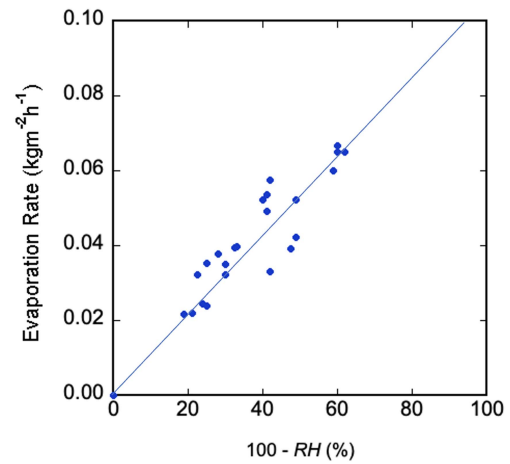**Fig. 4.** Saturation concentration x_{sat} of water vapor in air [Engineering Toolbox 2004].

Fig. 5. Steady-state evaporation rate ($t > 1$ h) of deionized water from half-filled beakers at 23 °C as a function of ambient relative humidity.

0.049 kg·m^{-2}·h^{-1}, much smaller than expected from (4). The initial, transient evaporation rate of water is several times greater [Poulose 2023], although still less than predicted by the equation.

The average evaporation rate for water in the microchannel is approximately 0.132 kg·m^{-2}·h^{-1}, compared to 0.345 kg·m^{-2}·h^{-1} given by (4) at 22 °C and RH $= 50\%$. When corrected for the temperature and humidity differences, the evaporation rate in the microchannel is about twice as fast as the evaporation rate from half-filled beakers [Poulose 2023], where the water also evaporates into its own vapor, but the air is unsaturated. The flow dynamics of water in the microchannel and in the beaker must be quite different. The flow regime in the two cases may be characterized by the inverse Bond number, the dimensionless ratio $(\partial g/\partial T)/\beta \rho g d^2$ of Marangoni to Rayleigh numbers, which reflects the relative importance of the surface tension and gravitational forces that influence the flow. Here, $\beta = 2.1 \times 10^{-4}$ K^{-1} is the thermal expansion coefficient of water, and d is the depth. The ratio is 316 000 for the microchannels and 90 for the beakers. Surface tension dominates flow in the channel. The faster evaporation rate of water in the microchannel compared with the beaker is attributed to Marangoni convection. Thermocapillary flow with the vortex pattern sketched in Fig. 1(c), like that observed at a meniscus in a capillary [Buffone 2005, 2014, Dhavaleswarapu 2007], will increase evaporation in the microchannel. A magnetic field is known to influence the flow in droplets of ferrofluids and conducting fluids [Dhar 2019, Jaiswal 2018], but deionized water is neither conducting nor magnetic.

The vapor close to the meniscus is composed of freshly evaporated molecules, which need high kinetic energy and well-timed making and breaking of at least three hydrogen bonds at the interface in order to break loose [Nagata 2015]. The isomer ratio of such water vapor may differ from that in liquid water, and its effective temperature will be higher than ambient in the channel, allowing it to evaporate without immediately recondensing. The Knudsen layer where there is a temperature gradient normal to the water surface [Jafari 2019] must be wide enough to allow evaporation to proceed into the channel at the ambient temperature of 26 °C.

In order to account for our results on evaporation of deionized water in microchannels, we must look for an effect of the magnetic field on the vapor, rather than on the liquid—specifically an effect on the isomer ratio. We developed this idea to explain the field effect in beakers, where the largest enhancement was 36%, and the average over 36 runs was $12\pm7\%$ [Poulose 2023]. By treating the *ortho* and *para* isomers of water vapor as independent gasses, each with its own partial pressure, we found that the *ortho* percentage in fresh vapor was $f_L^o = 39 \pm 1\%$. It approaches the equilibrium value of 75% in ambient air very slowly because transitions between the isomeric states are strongly forbidden [Abragam 1961, Chaplin 2021]. The vapor accumulating in the confined space in the microchannel on either side of the water droplet should therefore have the freshly evaporated composition. Treating the two isomers as independent gasses, we assume that the steady-state evaporation rate depends on a dimensionless sum of *ortho* and *para* contributions

$$g_0 = \left[f_L^o \left(1 - f_V^o\right) + f_L^p \left(1 - f_V^p\right) \right] \qquad (5)$$

where f^o and f^p are the *ortho* and *para* fractions. L refers to fresh vapor emanating from the liquid, and V refers to ambient vapor in the channel. For each isomer, the evaporation is supposed to depend on the product of an attempt frequency proportional to f_L, the vapor fraction that accumulates at the liquid surface, and a success rate proportional to $(1 - f_V)$ that reflects the capacity of the air to absorb the isomer. The mass evaporation rate will then be given by g_0 and a multiplicative prefactor Q' that depends on a series of unknowns including liquid flow, surface temperature, and vorticity. Unlike a free or sessile droplet, where the evaporation rate due to diffusion depends on its radius [Gelderblom 2022, Wilson 2023], the free surface area $2A$, radius of curvature R, and contact angle θ in the channel do not change significantly during evaporation and the in-field or no-field evaporation rates change little after 50 m (see Fig. 3). We can therefore express the mass evaporation rate in the channels in kg·m^{-2}·h^{-1} and compare to the rate from beakers.

When the liquid in the channel is evaporating entirely into its own vapor, $f_L^o = f_V^o$. Since $(f_L^o + f_L^p) = (f_V^o + f_V^p) = 1$, the evaporation rate is then proportional to

$$g_0 = 2f_L^o(1 - f_L^o) \qquad (6)$$

which is the green parabola plotted in Fig. 6. Note that when the isomers are indistinguishable, (5) or (6) reduces to (4), except for the prefactor. However, the measured evaporation is always a *net* rate, proportional to $(g_0 - c)$, where c is the dimensionless condensation rate of water vapor reentering the liquid. It follows that the net evaporation rate in zero field is proportional to the distance between the dashed blue line that denotes the recombination rate c, assumed to be independent of the isomer involved, and the green parabola. Initially, when the vapor has the 3:1 isomeric composition, it is the distance between the dashed blue line and the gray sloping line for $f_V^o = 0.75$ that determines the evaporation rate.

A magnetic field causes the hydrogen protons to precess at the Larmor frequency of 46 MHz·T^{-1}, regardless of the direction of travel of the water molecule in the gas phase. The two protons precess at
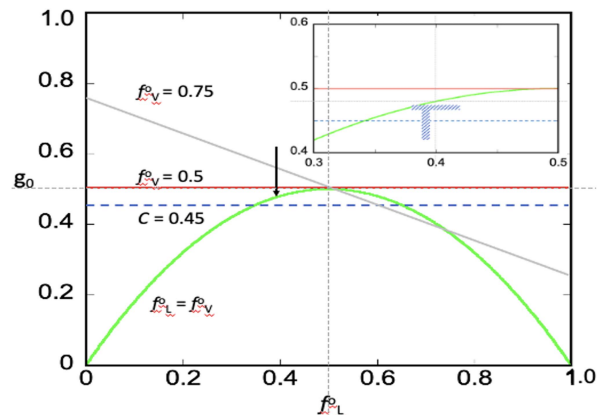

Fig. 6. Dimensionless evaporation rates of water as a function of the *ortho* fraction f_L^o present in the vapor escaping from the liquid for two cases. The parabolic green curve is for $f_L^o = f_V^o$, when the water is surrounded by its own vapor. The horizontal red line is for $f_V^o = 1/2$, after exposure to the magnetic field. The shaded areas in the insert mark ranges of f_L^o and recombination rate c (also red on the vertical axis) that are compatible with the field enhancement data.

slightly different frequencies in a nonuniform magnetic field, and the populations of the two isomers will be equalized as they become dephased so that each of them approaches $1/2$; $f_L^o = 1/2$ corresponds to the horizontal red line in the figure. Furthermore, Lorentz torque on the electric dipole moments of the water molecules also tends to increase f_V^o [Poulose 2023]. The key point is that the evaporation rate of pure water is *always increased by a magnetic field*.

For evaporation from beakers, we found $f_L^o = 39 \pm 1\%$ with recombination rate $c = 0.40$, denoted by the arrow in Fig. 6. To account for the greater magnetic field effects in the microchannels when the *ortho* isomer content is 39%, a slightly higher recombination rate in the range $0.42 < c < 0.47$ is required in the more confined environment. Otherwise, the range of magnetic field effects could be accounted for if $f_L^o = 40 \pm 2\%$ with $c = 0.47$.

V. CONCLUSION

The remarkable magnetic field enhancement of the evaporation rate of deionized water confined in microchannels is explained by its effect on the *ortho:para* ratio of the evaporated water vapor, treating the isomers as independent gasses. From the magnitude of the magnetic field enhancement, it is possible to fix both the isomeric ratio of fresh vapor and the recombination rate to within a few percent. Surprisingly, the average evaporation rate of water in a microfluidic channel where the relative humidity exceeds 100% is notably greater than it is in an open beaker where the vapor is unsaturated. This is likely due to thermocapillary flow in the channel.

Future work should aim to confirm the isomeric ratio of fresh water vapor by terahertz spectroscopy, and visualize Marangoni vortex flow in the channel by particle image velocimetry in a field; evidence of a Lorentz force would reveal any related charge flow.

Our results suggest that the conventional treatment of evaporating water vapor as a single gas needs to be reconsidered in confined spaces where advection is limited. There is a prospect of relating the *ortho-para* ratio of fresh vapor to hydrogen bonding in different aqueous solutions [Rana 2022]. Furthermore, a magnetic field may prove to be useful for applications where it is desirable to increase the evaporation rate of water in microscale porous media without raising the temperature [Yang 2020].

ACKNOWLEDGMENT

REFERENCES

Abragam A, *Principles of Nuclear Magnetism*. Oxford, U.K.: Clarendon, 1961.

Buffone C, Sefiane K, Christy J R E (2005), "Experimental investigation of self-induced thermocapillary convection for an evaporating meniscus in capillary tubes using micro–particle image velocimetry," *Phys. Fluids*, vol. 17, 052104, doi: 10.1063/1.1901688.

Buffone C, Minetti C, Boussemaere L, Roudgar M., De Coninck J (2014), "Marangoni convection in evaporating meniscus with changing contact angle," *Exp. Fluids*, vol. 55, pp. 1833–1842, doi: 10.1007/s00348-014-1833-2.

Chaplin M (2021), "Ortho and para water," [Online]. Available: https://water.lsbu.ac.uk/water/ortho_para_water.html

Chibowski E, Szcześ A (2018), "Magnetic water treatment, A review of the latest approaches," *Chemosphere*, vol. 203, pp. 68–75, doi: 10.1016/j.chemosphere.2018.03.160.

Chibowski E, Szcześ A, Hołysz L (2014), "Influence of magnetic field in the evaporation rate and surface tension of water," *Colloids Interfaces*, vol. 2, pp. 68–79, doi: 10.3390/colloids2040068.

Davoust L, Theisen J (2013), "Evaporation rate of droplet arrays within a digital microfluidic system," *Sensors Actuators B*, vol. 189 pp. 157–163, doi: 10.1016/j.snb.2013.02.071.

Dhar P (2019), "Thermofluidic transport in droplets under electromagnetic stimulus: A comprehensive review," *J. Indian Inst. Sci.*, vol. 99, pp. 105–119, doi: 10.1007/s41745-018-0088-y.

Dhavaleswarapu H K, Chamarthy P, Garimella S V, Murthy J Y (2007), "Experimental investigation of steady buoyancy-thermocapillary convection near an evaporating meniscus," *Phys. Fluids*, vol. 19, 082103, doi: 10.1063/1.2752477.

Dueñas J A, Weiland C, García-Selfa I, Ruíz-Rodríguez F J (2021), "Magnetic influence on water evaporation rate: An empirical triadic model," *J. Magn., Magn. Mater.*, vol. 539, 168337, doi: 10.1016/j.jmmm.2021.168377.

Engineering Toolbox (2004), "Evaporation from a water surface," [Online]. Available: https://www.engineeringtoolbox.com/evaporation-water-surface-d_690.html

Gelderblom H, Diddens C, Marin A(2022), "Evaporation-driven flow in sessile droplets," *Soft Matter*, vol. 18, pp. 8535–8553, doi: 10.1039/d2sm00931e.

Jafari P, Amritkar A, Ghasemi H (2019), "Temperature discontinuity at an evaporating water interface," *J. Phys., Chem. C*, vol. 124, pp. 1554–1559, doi: 10.1021/acs.jpcc.9b10838.

Jaiswal V, Dwivedi R K, Harikrishnan A R, Dhar P (2018), "Magnetohydrodynamic- and magnetosolutal-transport-mediated evaporation dynamics in paramagnetic pendant droplets under field stimulus," *Phys. Rev. E*, vol. 98, 013109, doi: 10.1103/PhysRevE.98.013109.

Mamrashev A A, Maximov L V, Nikolaev N A, Chapovsky P L (2018), "Detection on nuclear spin isomers of water molecules by terahertz time-domain spectroscopy," *IEEE Trans. Terahertz Sci. Tech.*, vol. 8, no. 1, pp. 13–18, doi: 10.1109/TTHZ.2017.2764385.

Mammoli D, Salvi N, Milani J, Buratto R, Bornet A, Sehgal A A, Canet E, Pelupessy P, Carnevale D, Jannin S, Bodenhausen G (2015), "Challenges in preparing, preserving and detecting *para*-water in bulk: Overcoming proton exchange and other hurdles," *Phys. Chem. Chem. Phys.*, vol. 17, pp. 26819–26827, doi: 10.1039/C5CP03350K.

Nakagawa J, Hirota N, Kitazawa, K, Shoda M (1999), "Magnetic field enhancement of water evaporation," *J. Appl. Phys.*, vol. 86, pp. 2923–2926, doi: 10.1063/1.371144.

Nagata Y, Usui K, Bonn M (2015), "Molecular mechanism of water evaporation," *Phys. Rev. Lett.*, vol. 115, 236102, doi: 10.1103/PhysRevLett.115.236102.

Poulose S, Venkatesan M, Möbius M, Coey J M D (2023), "Evaporation of water and urea solutions in a magnetic field; The role of nuclear isomers," *J. Colllloid Interface Sci.*, vol. 629, pp. 814–824, doi: 10.1016/j.jcis.2022.09.021.

Rana B, Fairhurst D J, Jena K C (2022), "Investigation of water evaporation process at air/water interface using Hofmeister ions," *J. Amer. Chem. Soc.*, vol. 144, pp. 17832–17840, doi: 10.1021/jacs.2c05837.

Wilson S K, D'Ambrosio H-M (2023), "Evaporation of sessile droplets," *Ann. Rev. Fluid Mech.*, vol. 55, pp. 481–509, doi: 10.1146/annurev-fluid-031822-013213.

Yang K, Ye G, De Schutter G (2020), "Will ortho-enriched water increase the durability of concrete?," in *Proc. 4th Int. RILEM Conf. Microstructure-Related Durability Cementitious Composites*, pp. 713–720. [Online]. Available: https://pure.tudelft.nl/ws/files/102482002/Will_ortho_enriched_water_increase_the_durability_of_concrete.pdf

Yang Q-W, Wei H, Li Z (2021), "Enhancing water evaporation by combining dynamic and static treatment," *Desalination Water Treat.*, vol. 216, pp. 299–305, doi: 10.5004/dwt.2021.26829.

Zhang C, Zhou Y, Shao T, Xie Q, Xu J, Yang W (2014), "Hydrophobic treatment on polymethylmethacrylate surface by nanosecond-pulse DBDs in CF_4 at atmospheric pressure," *Appl. Surf. Sci.*, vol. 311, pp. 468–477, doi: 10.1016/j.apsusc.2014.05.091.